Journal of the European Ceramic Society 17 (1997) 599–613

PII: S0955-2219(96)00112-4
0955-2219/97/$17.00

Effect of Starting Composition, Type of Rare Earth Sintering Additive and Amount of Liquid Phase on $\alpha \rightleftarrows \beta$ Sialon Transformation

Necip Camuşcu,[a] Derek P. Thompson[a] & Hasan Mandal[b]

[a]Materials Division, Department of Mechanical, Materials and Manufacturing Engineering, University of Newcastle upon Tyne, NE1 7RU, UK
[b]Department of Ceramic Engineering, Anadolu University, Eskisehir, Turkey

(Received 8 January 1996; revised version received 30 May 1996; accepted 11 June 1996)

Abstract

Five different α-β *sialon and* α*-sialon compositions have been prepared using different rare earth oxide additives namely, neodymium, samarium, dysprosium and ytterbium. Post-sintering heat treatments have been carried out at 1450°C for up to 720 h (one month) to observe* α → β *sialon transformation. A combination of X-ray and microstructural observations has shown that the high-temperature stability of the* α*-sialon phase depends on the starting composition, the type of rare earth sintering additives, the amount and viscosity of the liquid phase, and the presence or absence of* β*-sialon grains in the initial sintered material.* © *1997 Elsevier Science Limited. All rights reserved.*

1 Introduction

Sialon ceramics are one of the advanced structural ceramics at present being developed for high-temperature engineering applications. Because of their unique combination of properties they are ideal for the development of some areas of high technology especially in the mechanical, chemical, metallurgical, automotive and defence industries.

There are two different sialon phases, β with the formula $Si_{6-z}Al_zO_zN_{8-z}$ where $z \leq 4{\cdot}0$ and α with the formula $M_xSi_{12-(m+n)}Al_{(m+n)}O_nN_{16-n}$, where M is a metal ion typically Li, Mg, Ca, Y and Ln where $Z \geq 58$. The β-sialon phase forms with more elongated grains and thereby increases the fracture toughness compared to the α-sialon phase which forms with relatively small, hard, equiaxed grains. Thus, the mechanical properties are very strongly dependent on the $\alpha:\beta$ sialon ratio and therefore optimized mechanical properties of sialon ceramics can be achieved very precisely in mixed α-β sialon composites.[1,2]

Recently, it has been shown by Mandal and co-workers[3–5] that the phase content of certain α-β sialon compositions can be greatly affected by heat-treatment procedures when rare earth oxides are used as the sintering aid. It has been observed that the α-sialon phase is less stable at low temperatures and decomposes into rare-earth-rich intergranular phase(s) and β-sialon with a remarkably elongated crystal morphology. The extent of the transformation is more pronounced with increased heat-treatment temperature. It was also pointed out by the same authors that the transformation is fully reversible.[6]

This transformation provides an excellent mechanism for optimizing phase content and microstructure without further additions of oxides and nitrides merely by heat-treatment at appropriately chosen temperatures. In this way predetermined values of hardness, strength and toughness can be achieved from a single starting composition.

While materials prepared in this way can obviously be used successfully below the transformation temperature of the glass (≈1000°C), many applications for α-β sialon ceramics are in the range 1000–1300°C, and it is clear from the above discussion that $\alpha \rightarrow \beta$ sialon transformation will continue during use of the materials with consequent continuous change in properties.[7] A complete understanding of the mechanism of this interesting transformation is therefore essential to define more precisely safe operating conditions for sialon ceramics.

Several mechanisms have been previously considered by the same authors to explain the $\alpha \rightleftarrows \beta$ sialon transformation observations described above. These are discussed below.

1.1 Surface effects

It is not uncommon in mixed α-β sialon ceramics to find a different $\alpha:\beta$ sialon ratio in the centre of

the sample compared with the outside. However, earlier work[3] has shown that there was no difference between the inside and outside of the sample in $\alpha \rightarrow \beta$ sialon transformed material.

1.2 Change of composition during sintering

Also, it is not uncommon in mixed α-β sialon ceramics to find a different $\alpha:\beta$ sialon ratio in the final product compared with that expected from the starting composition. This arises from milling additions, effect of furnace atmosphere, weight loss, etc. However, the phenomenon described in this transformation changes with temperature and is also reversible.[3,6]

1.3 Phase relationships

An obvious alternative explanation for $\alpha \rightarrow \beta$ sialon transformation is in terms of phase relationships. The shape of the liquid phase region changes as a function of Ln content, Si : Al and O : N ratios and temperature. The increased N, Al, Ln content of liquid phase at high temperature would promote a decrease in $\alpha:\beta$ sialon ratio with increasing temperature. Moreover the effect would be expected to show a uniform change with temperature, whereas the present observations show an increase in β-sialon content up to ≈ 1550°C and an increase in α-sialon above this temperature.[3,8] From the above discussion, it is clear that even though phase relationships play some part in $\alpha \rightarrow \beta$ sialon transformation, they are not sufficient to account for the observed behaviour.

1.4 Effect of cation size

Since the original work showed that transformation was more apparent when high atomic number rare earth sintering additives (Yb_2O_3) were used, the transformation was originally believed to be due to the smaller rare earth cations being large enough to occupy the interstices in the α-sialon structure at high temperature but too small at lower temperatures so that the α-sialon structure became unstable.[3] However, later results showed that sialon compositions densified with large cation size sintering additives also showed similar transformation effects.

In the present work, α-sialon and α-β sialon starting compositions have been densified by either hot-pressing or pressureless sintering using Ln_2O_3 additives where Ln is neodymium, samarium, dysprosium and ytterbium. The resulting materials have been heat-treated at 1450°C for up to one month to observe the transformation. The pre-prepared glass powders were also added to certain compositions to see the effect of liquid phase.

The effects of different cation size, α-sialon composition, the amount and viscosity of liquid phase and the presence of β-sialon have been discussed.

2 Experimental

Four rare earth elements, Nd, Sm, Dy and Yb were selected for the preparation of α and α-β sialon ceramics. The starting compositions in different systems are given in Table 1, and the relevant chemical formulation, and graphical representation of the starting compositions are shown in Fig. 1. The reasons for choosing these compositions are explained in Sections 3.1 and 3.2. Although the weight percentage of rare earth oxides increases a little as the atomic number of lanthanide elements increases, in mole ratio, the amount of Ln_2O_3 in different samples is exactly the same.

Sialon compositions were prepared using powder mixtures of Si_3N_4 (HC Stark, Berlin, Grade LC10), AlN (HC Stark, Berlin, Grade A), Al_2O_3 (Alcoa, Grade A16SG), Ln_2O_3 (99·9%, Sigma Chemical Company Ltd). The rare earth oxides were calcined at 1000°C for 4 h before use, to remove any absorbed water. When calculating the compositions, 3·5% SiO_2 and 3·5% Al_2O_3 (according to manufacturer's specifications) on the surfaces of Si_3N_4 and AlN respectively were taken into account.

The starting materials were mixed in water-free isopropanol and milled in an agate mortar for 45 min. This method was used to avoid segregation of rare earth oxides during drying. The size of batch used was 15 g. After drying and sieving, powders were compacted into pellets (about 3 g) by pressing uniaxially and then isostatically under 200 MPa. Before firing, the specimens were embedded in micron-sized boron nitride powder in graphite crucibles and sintered in a carbon

Table 1. Starting compositions of different Ln_2O_3 densified α-β and α-sialon ceramics

Composition	*Formulation*	*Si_3N_4*	*Al_2O_3*	*AlN*	*Ln_2O_3*
Ln1	$Ln_{0.053}Si_{1.77}Al_{0.234}O_{0.333}N_{2.43}$	83·38	5·14	5·47	8·94 (Nd_2O_3) or 9·27 (Sm_2O_3) or 9·90 (Dy_2O_3) or 10·46 (Yb_2O_3)
Ln2	$Ln_{0.053}Si_{1.782}Al_{0.235}O_{0.264}N_{2.49}$	83·73	3·10	7·18	8·94 (Nd_2O_3) or 9·27 (Sm_2O_3) or 9·90 (Dy_2O_3) or 10·46 (Yb_2O_3)
Ln3	$Ln_{0.053}Si_{1.741}Al_{0.287}O_{0.229}N_{2.51}$	82·08	1·23	10·74	8·94 (Nd_2O_3) or 9·27 (Sm_2O_3) or 9·90 (Dy_2O_3) or 10·46 (Yb_2O_3)
Ln4	$Ln_{0.333}Si_{9.3}Al_{2.7}O_{1.7}N_{14.3}$	71·82	3·40	15·55	9·23 (Nd_2O_3) or 9·57 (Sm_2O_3) or 10·24 (Dy_2O_3) or 10·83 (Yb_2O_3)
Ln5	$Ln_{0.5}Si_{9.0}Al_{3.0}O_{1.5}N_{14.5}$	66·77	2·02	17·93	13·29 (Nd_2O_3) or 13·78 (Sm_2O_3) or 14·75 (Dy_2O_3) or 15·58 (Yb_2O_3)

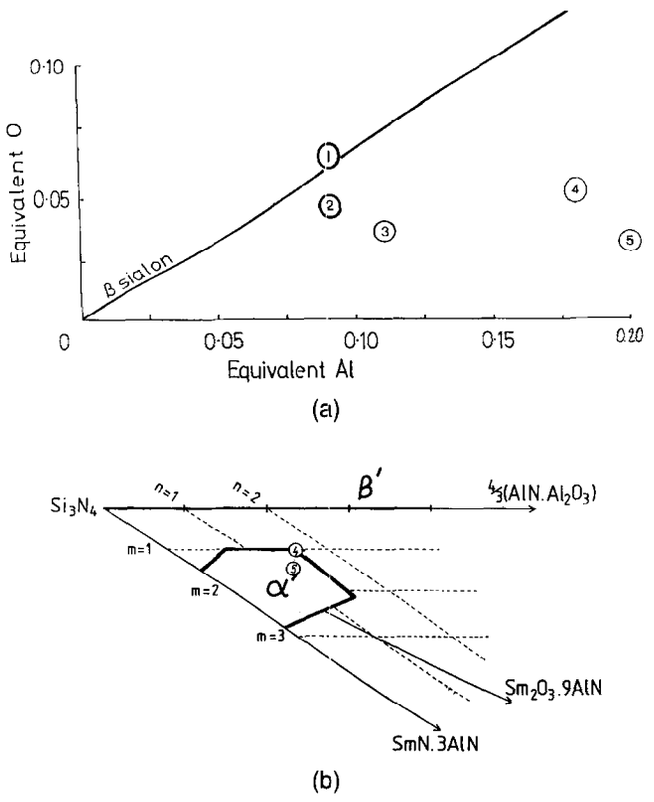

Fig. 1. (a) Overall starting compositions represented as equivalents of oxygen and aluminium added to silicon nitride (b) the α-sialon plane, showing the Ln4 and Ln5 compositions used in this study.

resistance furnace at 1800°C for 2 h under a protective nitrogen atmosphere and then the furnace was cooled at a rate of 50°C min^{-1} from 1800 to 1200°C. The green pellets were also hot pressed in BN-coated graphite dies at 1800°C for 1 h.

Additions of 10 and 20 wt% of glass powders with an overall composition Ln : Si : Al = 1 : 1 : 1 and O : N = 6 : 1[9] were made to certain sialon starting compositions and mixed powders were pressureless sintered at 1800°C.

All sintered materials were placed in a carbon crucible and re-heated up to 1800°C in a smaller size pressureless sintering furnace for 20 min and quenched (400°C min^{-1}) to room temperature. Heat-treatment was carried out for all samples in an alumina tube furnace at 1450°C for up to 720 h (one month) under a nitrogen gas atmosphere.

Product phases were characterized by X-ray diffraction (XRD) using a Hägg-Guinier camera and Cu$K\alpha_1$ radiation. The computer-linked line scanner (SCANPI LS-20) system, developed by Werner (Arrhenius Laboratory, University of Stockholm, Sweden) was used for direct measurements of X-ray films and refinement of lattice parameters. The amounts of α- and β-sialon phases were found by quantitative estimation from the XRD pattern using the integrated intensities of the (102) and (210) reflections of α-sialon and the (101) and (210) reflections of β-sialon in the following equation:

$$\frac{I_\beta}{I_\alpha + I_\beta} = \frac{1}{1 + K[(1/W_\beta) - 1]} \quad (1)$$

where I_α and I_β are observed intensities of α- and β- sialon lines respectively, W_β is the relative weight fraction of β-sialon and K is the combined proportionality constant resulting from the constants in the two equations, namely:

$$I_\beta = K_\beta * W_\beta \quad (2)$$

$$I_\alpha = K_\alpha * W_\alpha \quad (3)$$

which is 0·518 for β(101) - α(102) reflections and 0·544 for β(210) - α(210) reflections.[10]

After application of a gold coating, polished surfaces of as-sintered and heat-treated samples were examined using a Camscan S4-80 DV scanning electron microscope (SEM) equipped with EDX facilities and a windowless detector suitable for light-element analysis

3 Results

3.1 Ln1, Ln2 and Ln3 starting compositions

As can be seen from Fig. 1, these compositions were designed to produce mixed α-β sialon phases after sintering. The reasons for choosing these compositions were as follows:

(a) Ln1 is the original starting composition used in previous work which has been shown to readily undergo α ⇄ β sialon transformation,[3]
(b) Ln2 is in the two-phase region (≈ 30% α-sialon and 70% β-sialon),
(c) Ln3 is also in the two-phase region but is more α-sialon rich (≈ 50% α-sialon and 50% β-sialon). This composition was useful to compare with both Ln1 and Ln2 compositions to understand the effect of liquid phase, since the amount of liquid is less and the viscosity is higher than in the other two compositions.

Examination of polished cross-sections of the sintered samples by SEM showed only very few micro-pores to be present, indicating that the samples had reached virtually theoretical density by pressureless sintering. In all sintered and subsequently quenched samples, there were no crystalline phase(s) at grain boundaries. The relative amounts of α- and β-sialon phases after quenching were established by XRD and the results are presented in Fig. 2.

Although different starting compositions were used with the intention of producing different

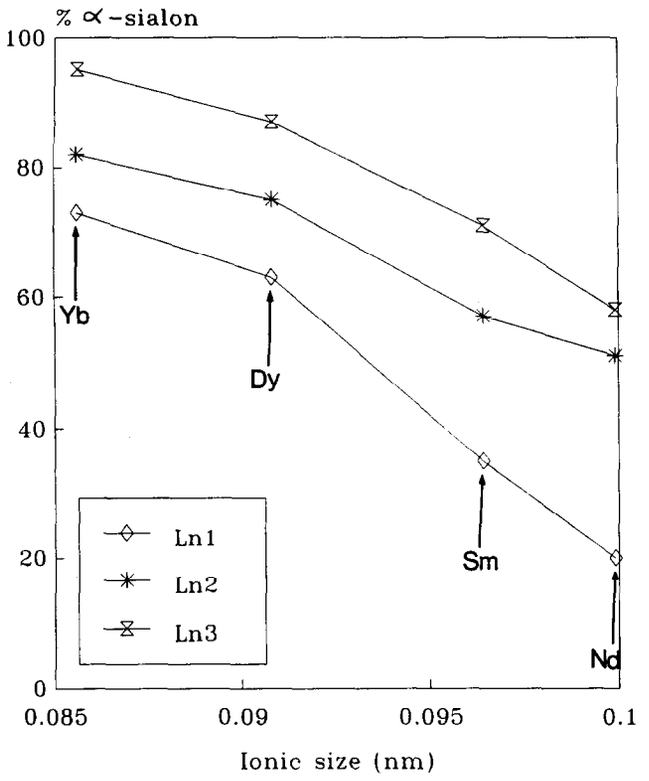

Fig. 2. α:(α+β) Sialon ratio of Ln1, Ln2 and Ln3 compositions after fast cooling, expressed in terms of size of rare earth cation.

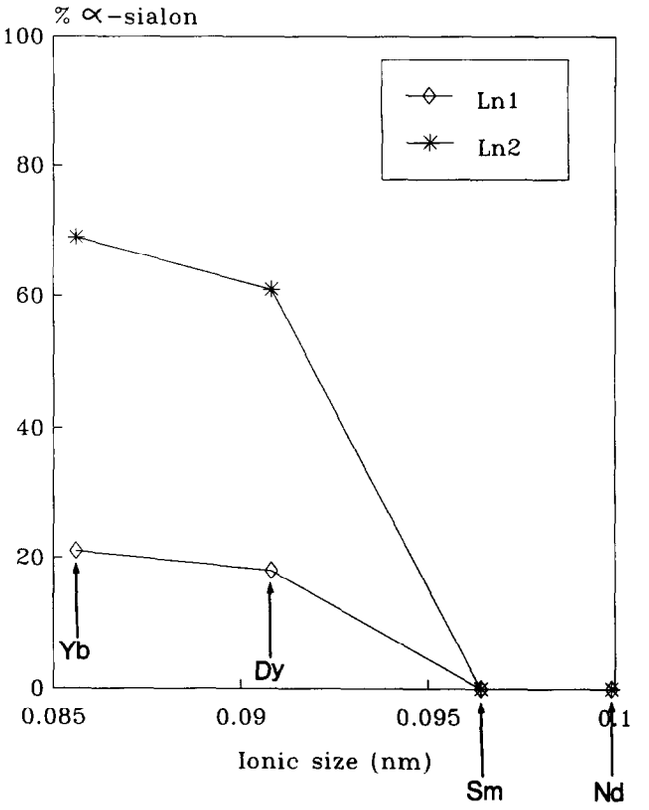

Fig. 3. α:(α+β) Sialon ratio of Ln1 and Ln2 compositions after 24 h heat-treatment at 1450°C.

amounts of α- and β-sialons, only Nd_2O_3- and Sm_2O_3-densified samples gave results close to the predetermined $\alpha:\beta$ sialon ratio while Yb_2O_3- and Dy_2O_3-densified samples gave very nearly the same amount of α-sialon after sintering (e.g. 73%, 82% and 95% α-sialon for Ln1, Ln2 and Ln3 compositions respectively in Yb_2O_3 samples).

Post-sintering heat-treatment experiments were carried out at 1450°C for up to 168 h (one week) in order to study the effects of prolonged heat treatments on $\alpha \rightarrow \beta$ sialon transformation. XRD results are given in Fig. 3 as a comparison between Ln1 and Ln2 compositions after 24 h heat-treatment at 1450°C; and in Fig. 4 as a comparison between Ln1, Ln2 and Ln3 compositions after 168 h of heat treatment at the same temperature.

As can be clearly seen from both figures, although the amounts of α- and β-sialon phases were very nearly the same after sintering when Yb_2O_3 and Dy_2O_3 were used as the sintering additives, the amounts were significantly different after heat-treatment. Sample Yb1 showed nearly full transformation while Yb2 showed only 10% transformation at the end of 24 h heat treatment. However, the amount of α-sialon in sample Yb2 was significantly reduced to 40% when the heat-treatment time increased from 24 h to 168 h. Under the same conditions the amount of α-sialon in sample Yb3 was only reduced from 95% to 80%.

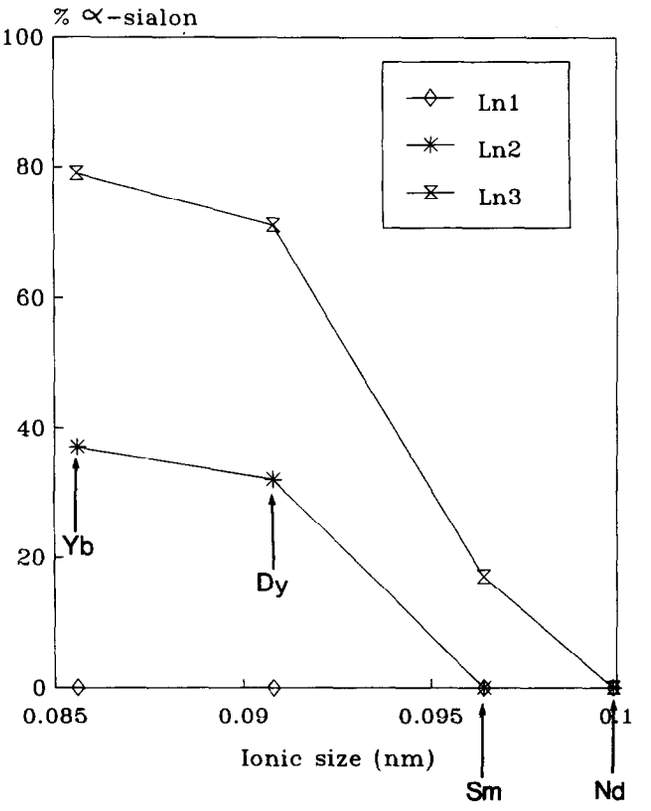

Fig. 4. α:(α+β) Sialon ratio of Ln1, Ln2 and Ln3 compositions after 168 h heat-treatment at 1450°C.

A similar effect has also been seen in Dy_2O_3-densified samples. The Nd- and Sm-systems showed a greater tendency for $\alpha \rightarrow \beta$ sialon transformation

since the ionic radii of these cations are larger than those of Dy- and Yb-. Therefore the formation of α-sialon became more difficult during sintering and the excess rare earth cations went into the liquid phase, increasing the amount of liquid and reducing its viscosity. As a result, $\alpha \rightarrow \beta$ sialon transformation became significantly faster and no α-sialon remained even in Ln3 samples after 168 h heat-treatment.

Figures 5 and 6 show typical back-scattered SEM images of Yb_2O_3-densified samples after sintering and after different heat-treatment experiments respectively. Since the contrast on back-scattered electron micrographs depends mainly on the mean atomic number, micrographs very clearly distinguish between the various phases; the β-sialon and 21R grains (which contain no rare earth element) are black and more needlelike, whereas the α-sialon grains (which contain a small amount of rare earth element) are grey and more equiaxed, whilst Ln-rich crystalline or glassy phases appear fine-grained and white, because of the high Ln content.

Although the X-ray results showed very similar amounts of α- and β-sialon phases in the Yb_2O_3 samples, SEM micrographs clearly indicate the difference between the three compositions in terms of grain-boundary phases (white areas) which are present in nearly twice the amount in Ln1 as compared to Ln2.

Systematic differences were observed by SEM on moving to lower Z rare earth additives, namely, that the α-sialon content decreases, and the amount of intergranular phases increases. The explanation for the decrease in α-sialon content correlates with the relative sizes of the rare earth metal dopants of the sintering additives, so that ytterbium and dysprosium form more α-sialon whereas neodymium and samarium form less α-sialon. Clearly, the explanation for the increase in the amount of intergranular phase for low atomic number rare earth additives is related to the low α-sialon content, since α-sialons incorporate some of the densification additives(s) into the crystal structure, as a result of which the quantity of residual glass in the grain boundaries decreases with increasing α-sialon content. Therefore the amount of residual glass in samples densified with Dy_2O_3 and Yb_2O_3 additives is considerably less than in Sm_2O_3- and especially Nd_2O_3-densified compositions.

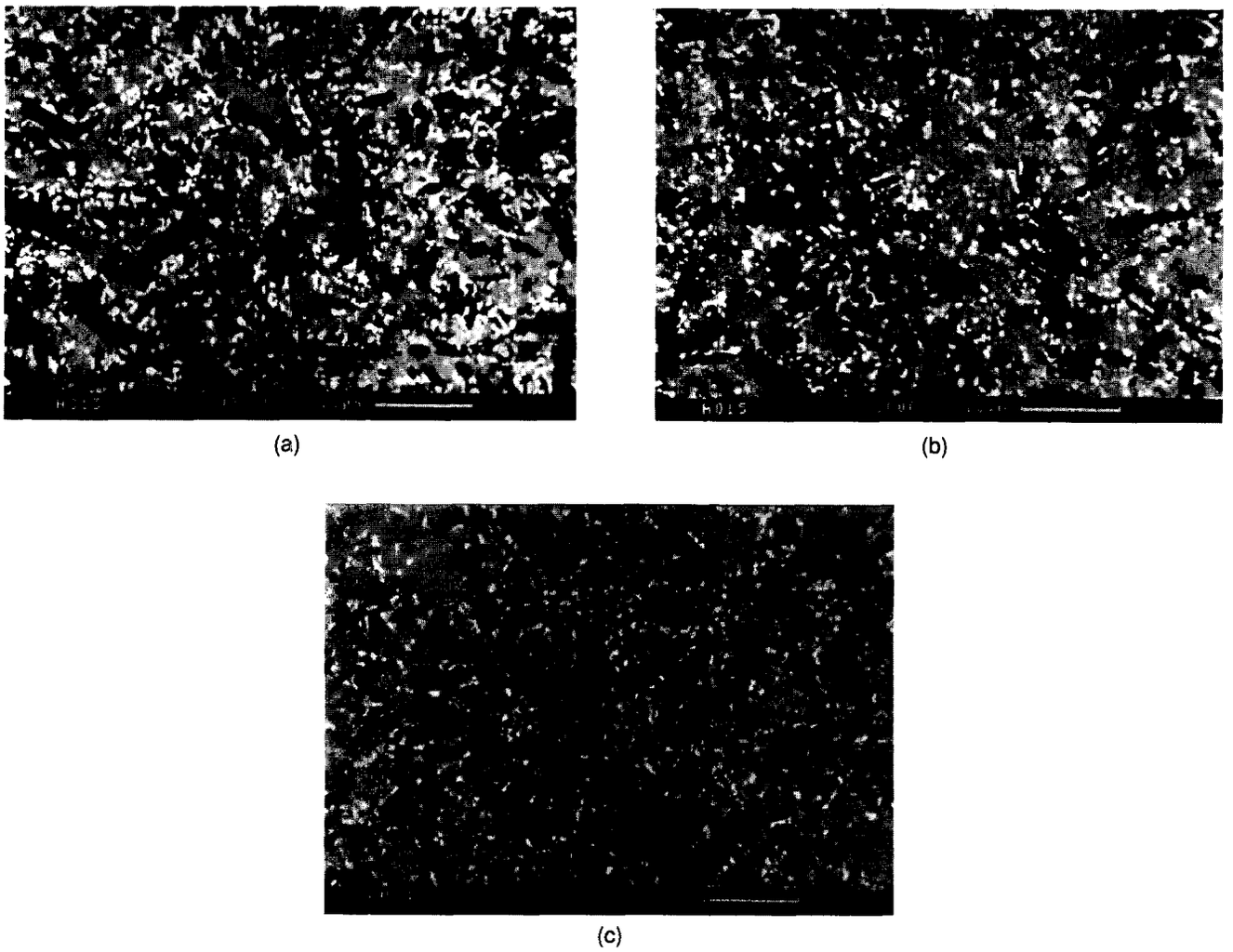

Fig. 5. Back-scattered SEM micrographs of the Yb_2O_3-densified samples after fast cooling: (a) Ln1, (b) Ln2 and (c) Ln3.

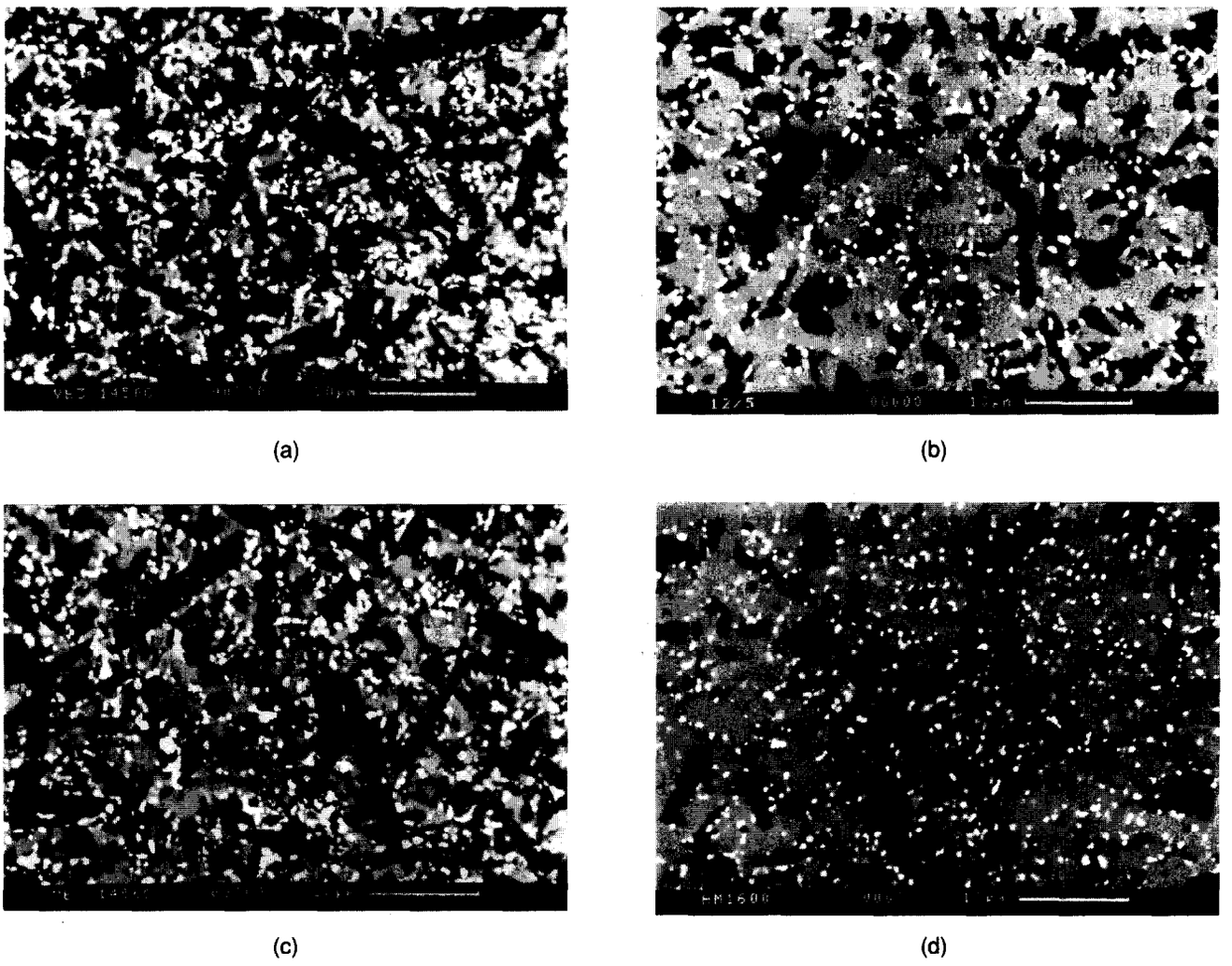

Fig. 6. Back-scattered SEM micrographs of the Yb_2O_3-densified samples after heat-treatment at 1450°C for 24 h: (a) Ln1, (b) Ln2 and for 168 h: (c) Ln2 and (d) Ln3.

These results clearly show that more oxygen-rich α-sialons, such as the one present in the Ln1 composition, transform to β-sialon more readily than nitrogen-rich α-sialons, typified by the one present in the Ln3 composition.

Further experiments have been carried out by adding 10% and 20% of glass powders of overall composition Ln : Si : Al = 1 : 1 : 1 and O : N = 6 : 1 ($Ln_3Si_3Al_3O_{12}N_2$ - U-phase) to the Yb3 sample (which originally showed very little transformation). The XRD and SEM results of as-sintered and heat-treated samples are given in Figs 7 and 8 respectively. The rate of transformation became very significant for samples with additional amounts of glass powder and therefore all the α-sialon in Samples Yb3G10 and Yb3G20 transformed into β-sialon at the end of 168 h. These results for added liquid phase clearly show that a most important factor influencing the transformation is the amount and viscosity of liquid present during heat-treatment and therefore the overall equation representing $\alpha \rightarrow \beta$ sialon in Ln1, Ln2 and Ln3 type of starting compositions is as follows regardless of the type of sintering additive:

$$\alpha\text{-sialon} + \beta\text{-sialon} + (21R) + \text{liquid} \rightarrow \beta\text{-sialon} + (21R) + \text{grain-boundary phase(s)} \quad (4)$$

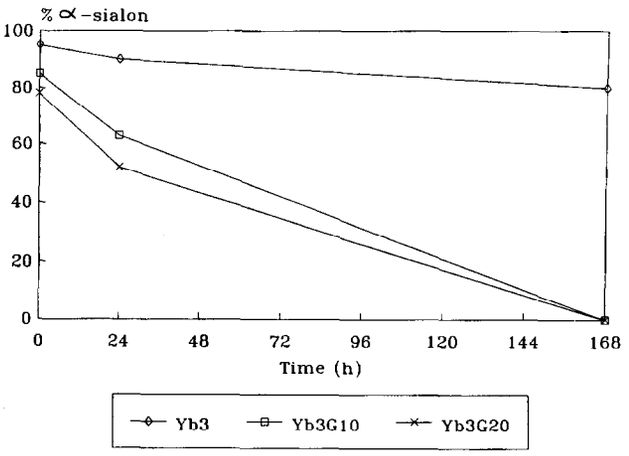

Fig. 7. α-Sialon content for Yb3 sample with 10% and 20% of glassy phase varying heat-treatment time at 1450°C.

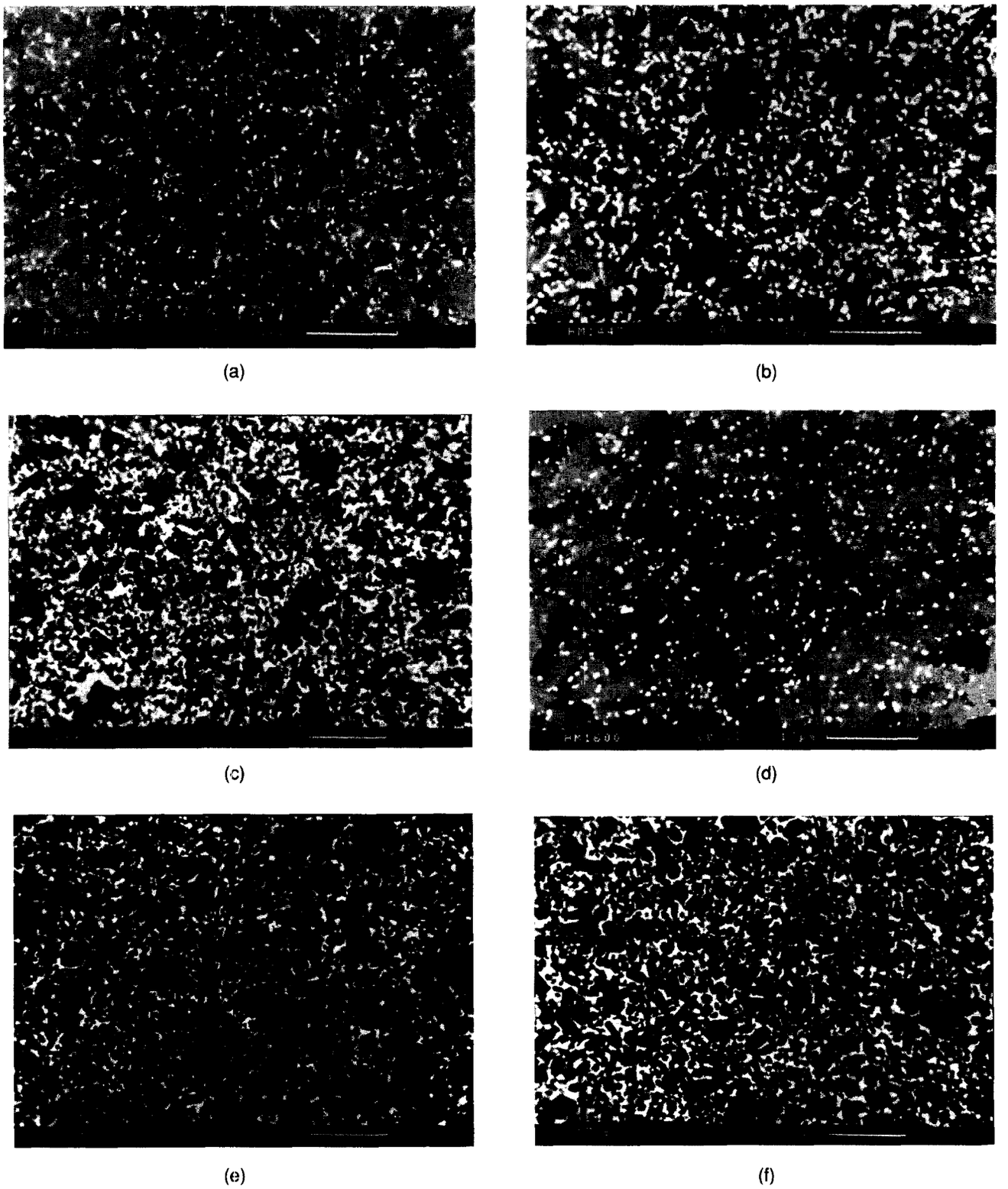

Fig. 8. Back-scattered SEM micrographs of fast-cooled samples: (a) Yb3, (b) 90% Yb3 + 10% glass, (c) 80% Yb3 + 20% glass and after heat-treatment at 1450°C for 168 h (d) Yb3 (e) 90% Yb3 + 10% glass, (f) 80% Yb3 + 20% glass.

3.2 Ln4 and Ln5 starting compositions

Graphical representation of these starting compositions, which were designed to produce 100% α-sialon after sintering, is given in Fig. 1(b). The reasons for selecting these specific compositions were as follows:

(a) Ln4, an α-sialon composition with $m = 1$ and $n = 1{\cdot}7$, is located at the oxygen-rich corner of the α-sialon phase region and is designed to determine whether all different cation size rare earth oxide sintering additives give pure α-sialon, since the borders of the α-sialon phase region have only been established precisely in the yttrium system.[11]

(b) Ln5, an α-sialon composition with $m = 1{\cdot}5$ and $n = 1{\cdot}5$, is inside the α-sialon phase region and is almost the maximum nitrogen

Table 2. Densities of Ln4 and Ln5 composition sintered at 1800°C by hot-pressing

Composition	*Densities (g/cm³)*			
	Nd_2O_3	Sm_2O_3	Dy_2O_3	Tb_2O_3
Ln4	3·354	3·367	3·378	3·398
Ln5	3·445	3·466	3·503	3·543

content α-sialon composition which can be prepared without LnN, (which is expensive and cannot be handled easily because of hydrolysis).

Hot pressing techniques have been used for sintering these compositions since it is very difficult to obtain full densification of pure α-sialon compositions by pressureless sintering. A comparison of the effectiveness of rare-earth sintering additives on the densification of α-sialon ceramics has been recently reported elsewhere.[12]

The measured density of the hot-pressed samples showed a linear increase with increasing rare earth content as expected; the results are given in Table 2.

3.2.1 Ln4 compositions

The relative amounts of α- and β-sialon phases after sintering and heat-treatment were established by XRD and the results are presented in Table 3 and Fig. 9. In all sintered samples, α-sialon is the predominant phase and no other crystalline phase(s) appeared in the grain boundaries. Although all starting compositions aimed to produce 100% α-sialon, only Dy_2O_3 and Yb_2O_3 additions gave results close to the designed composition, while

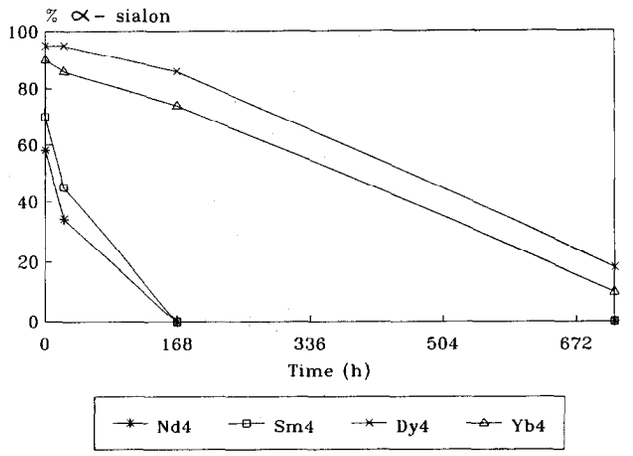

Fig. 9. α-Sialon content of Ln4 composition, expressed in terms of heat-treatment time.

Nd_2O_3 and Sm_2O_3 additions gave only ≈50% and ≈75%, α-sialon respectively. Since weight losses during hot pressing were negligible and the surface oxides on the Si_3N_4 and AlN were taken into account during preparation, the chemical instability of Nd- and Sm- α-sialon must be explained in terms of ionic size and therefore further work is needed to establish the extent of the α-sialon-forming regions in these systems.

X-ray results of heat-treated samples showed that α-sialon, β-sialon and 21R are the predominant phases. In addition, M'-phase in the neodymium and samarium systems; and garnet+J phases in the dysprosium and ytterbium systems were observed with an increasing amount of $\alpha \rightarrow \beta$ sialon transformation occurring along the lines of eqn (4).

It is very clear from the results that neodymium and samarium α-sialons readily undergo this

Table 3. X-ray results of sintered and heat-treated Ln4 samples

Sample	*HT time (h)*	*α' (%)*	*β' (%)*	*Other*
Nd4	Sint	m(58)	m(42)	21R(w)
	24	mw(15)	s(85)	21R(w), M'(w)
	168	0	vs(100)	21R(mw), M'(mw)
	720	0	vs(100)	21R(mw), M'(m)
Sm4	Sint	s(70)	mw(30)	21R(w)
	24	m(45)	m(55)	21R(w), M'(w)
	168	0	vs(100)	21R(mw), M'(mw)
	720	0	vs(100)	21R(mw), M'(m)
Dy4	Sint	vs(95)	vw(5)	21R(w)
	24	vs(95)	vw(5)	21R(w), G(vw), J(vw)
	168	s(86)	w(14)	21R(w), G(w), J(w)
	720	w(18)	s(82)	21R(w), G(mw), J(mw)
YB4	Sint	vs(91)	vw(9)	21R(w)
	24	s(86)	w(14)	21R(w), G(vw), J(vw)
	168	s(78)	mw(22)	21R(w), G(w), J(w)
	720	vw(10)	s(90)	21R(w), G(mw), J(mw)

Note: for X-ray peak intensities, s = strong, m = medium, w = weak, v = very; numbers in parentheses are relative percentages of α- and β-sialon phases. α' and β' = α and β-sialons; 21R = sialon polytypoid; M' = N-melilite solid solutions ($Ln_2Si_{3-x}Al_xO_{3+x}N_{4-x}$); G = $Ln_3Al_5O_{12}$; J = $Ln_4Si_2O_7N_2$.

Table 4. X-ray results of sintered and heat-treated Ln5 samples

Sample	*HT time (h)*	*α'(%)*	*β'(%)*	*Other*
Nd5	Sint	vs(97)	vvw(3)	21R(w)
	24	s(81)	w(19)	21R(w), M'(w)
	168	vw(8)	vs(92)	21R(mw), M'(m)
	720	0	vs (100)	21R(mw), M'(ms)
Sm5	Sint	vs(100)	0	21R(w)
	24	vs(100)	0	21R(w), M'(vvw)
	168	m(55)	m(45)	21R(mw), M'(w)
	720	0	vs(100)	21R(mw), M'(mw)
Dy5	Sint	vs(100)	0	21R(vw)
	24	vs(100)	0	21R(w), M' (vvw)
	168	vs(100)	0	21R(w), M' (vw)
	720	vs(100)	0	21R(w), M' (w)
Yb5	Sint	vs(100)	0	—
	24	vs(100)	0	G(vvw), J(vw)
	168	vs(100)	0	G(vw), J(w)
	720	vs(100)	0	G(mw), J(mw)

Note: for X-ray peak intensities, s = strong, m = medium, w=weak, v = very; numbers in parentheses are relative percentages of α- and β-sialon phases. α' and β' = α and β-sialons; 21R=sialon polytypoid; M'=N-melilite solid solutions ($Ln_2Si_{3-x}Al_xO_{3+x}N_{4-x}$); G=$Yb_3Al_5O_{12}$; J=$Yb_4Si_2O_7N_2$.

reaction. Although these additives produce M'-phase, which is an excellent grain-boundary phase for α- and α-β sialon ceramics at very high temperatures (1600°C),[13] M' formation is unfortunately accompanied by further $\alpha \rightarrow \beta$ sialon transformation which increases the amount of liquid phase present in the final ceramic. Therefore, in the neodymium and samarium compositions the α-sialon content gradually decreased as the heat treatment time increased and α-sialon had completely disappeared in both systems after 168 h (one week) at 1450°C. At the same time, the amount of M'-phase also increased even after the complete disappearance of α-sialon.

It is also clear from these results that the α-sialon phases in all these systems are unstable relative to β-sialon at 1450°C, but the rate of transformation varies markedly in the different systems. Thus, in the case of Dy- and Yb-systems, α-sialon was more stable than in the Nd- and Sm-systems, and after heat treatment for 168 h very little transformation is observed. However, the rate of transformation is nevertheless still on-going, and only $\approx$10 and $\approx$20% α-sialon remains in Yb- and Dy-samples respectively after 720 h (one month) of heat-treatment. In contrast, in the Nd- and Sm-systems, all the α-sialon phase had disappeared after one week (168 h) heat-treatment. The rate of transformation increases with the size of rare earth additive, and to some extent this is due to the fact that more liquid phase remains in these samples after cooling from the original sintering temperature. As already noted from the microstructures of these samples, the shape of residual glassy pockets in the high Z-samples is much more nearly spherical than in the low Z-samples, indicating improved wettability in the latter systems,[14] which is certainly another parameter promoting more rapid transformation. In the case of Dy- and Yb-systems, an additional factor is the very small number of β-sialon grains remaining after sintering, which then act as nucleation sites for the transformation. This point is discussed further in the next section.

3.2.2 Ln5 compositions

The results of sintered and heat-treated samples are given in Table 4 and Fig. 10. As seen from the table, 100% α-sialon, as designed, can be obtained for the sintering additives Sm_2O_3, Dy_2O_3 and Yb_2O_3. Although α-sialon was still the predominant phase when Nd_2O_3 was used as the sintering additive, some 3% β-sialon phase was also observed. The results also show that after prolonged

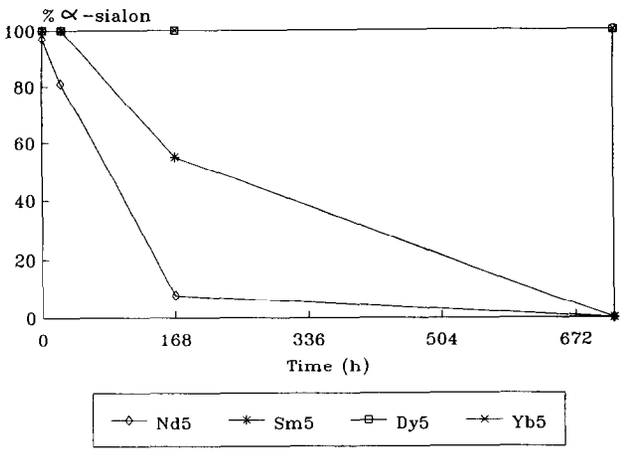

Fig. 10. α-Sialon content of Ln5 composition, expressed in terms of heat-treatment time.

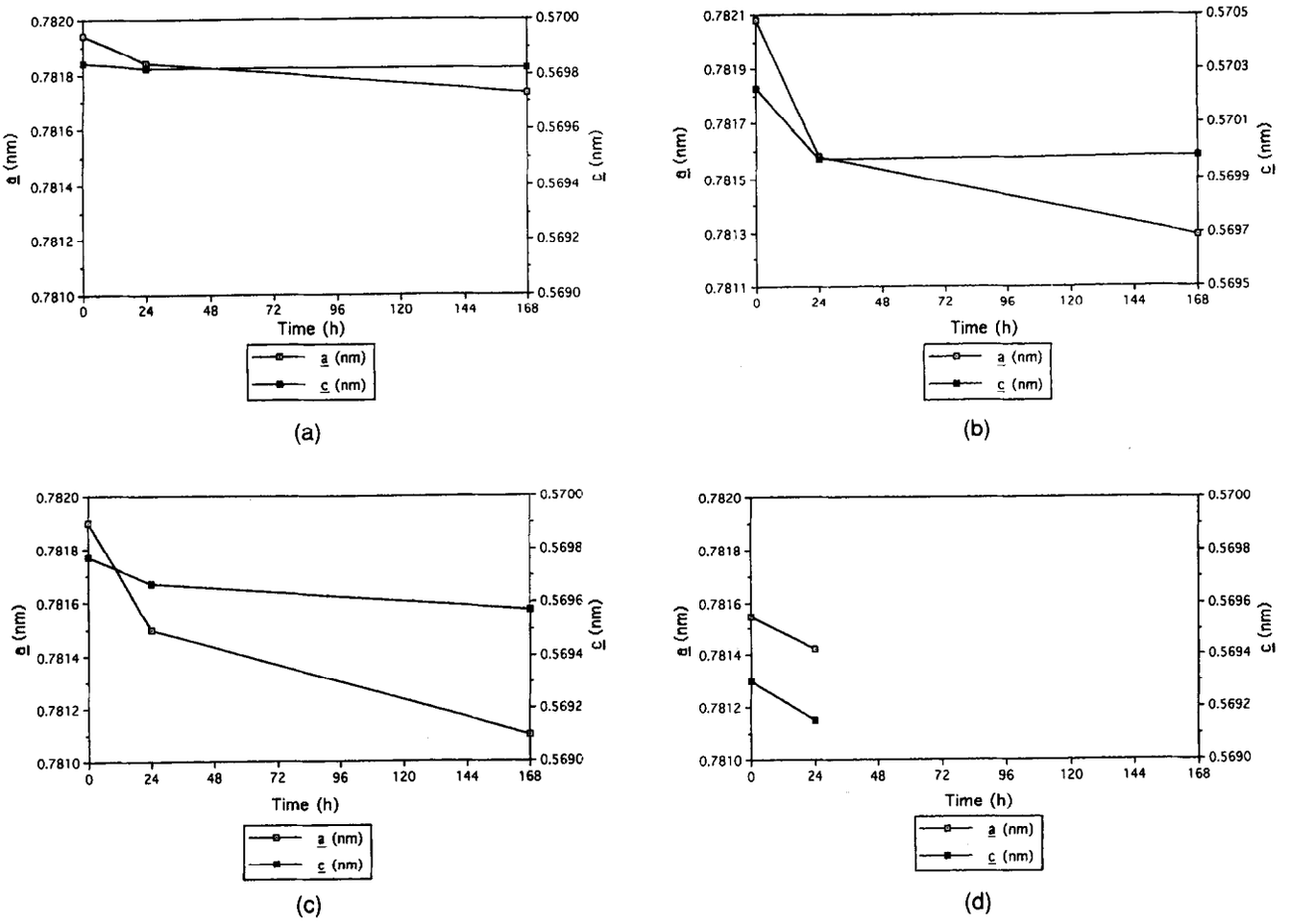

Fig. 11. Changes in unit cell dimensions of α-sialon phases with heat-treatment time for the samples of (a) Yb5, (b) Dy5, (c) Sm5 and (d) Nd5.

heat-treatment at 1450°C, there is a clear difference between the two groups (high and low atomic number) of rare earth sintering additives.

α-Sialon is the only matrix phase observed when Dy_2O_3 and Yb_2O_3 are used as additives; M' and J + garnet form respectively as the crystalline phases in these systems after heat treatment. Even after 720 h of heat-treatment at 1450°C, no $\alpha \rightarrow \beta$ sialon transformation was observed. The only change was a small increase in the amount of crystalline phases as a result of a decrease in the α-sialon unit cell dimensions during the first seven days of heat treatment; this latter trend stopped (see Fig. 11). The equation for this reaction is as follows:

$$\alpha_1\text{-sialon} + 21\text{R} + \text{liquid} \rightarrow \alpha_2\text{-sialon} + 21\text{R} + \text{crystalline phase(s) (M' or J+G)} \quad (5)$$

where α_1 is more dysprosium- or ytterbium-rich than α_2.

Although there was a clear sign of improvement in the thermal stability of neodymium and samarium α-sialons as compared with the results for α-sialon compositions with $m = 1$ and $n = 1{\cdot}7$ (Ln4 composition), the amount of α-sialon gradually decreased as the heat-treatment time increased and there was no α-sialon observed at the end of 720 h at 1450°C in both systems with an increasing amount of M'-phase as $\alpha \rightarrow \beta$ sialon transformation proceeded. In all systems, the composition of α-sialon also shifted towards lower rare earth contents but in Nd- and Sm-systems, the final α-sialon product transformed to β-sialon. The transformation reactions for these types of composition for large ionic size rare earth oxides are:

$$\alpha_1\text{-sialon} + \text{L}_1 + 21\text{R} \rightarrow \alpha_2\text{-sialon} + \beta\text{-sialon} + \text{M}' + 21\text{R} + \text{L}_2 \quad (6)$$

followed by:

$$\alpha_2\text{-sialon} + \beta\text{-sialon} + \text{M}' + 21\text{R} + \text{L}_2 \rightarrow \beta\text{-sialon} + \text{M}' + 21\text{R} + (\text{L}_3) \quad (7)$$

The microstructures of as-sintered and heat-treated Nd5 and Dy5 samples are shown in Fig. 12; the contrast between the β-sialon matrix for neodymium and the almost pure α-sialon matrix for dysprosium is clearly apparent after 168 h heat treatment at 1450°C although their sintered SEM micrographs are very similar. Another effect which comes out clearly from the micrographs is

that the small residual glassy pockets in the dysprosium sample take on a distinctly spherical shape and are all of very similar size; moreover, they are obviously not located at the grain boundaries between α-sialon grains. Clearly the residual liquid phase in this sample is not wetting the

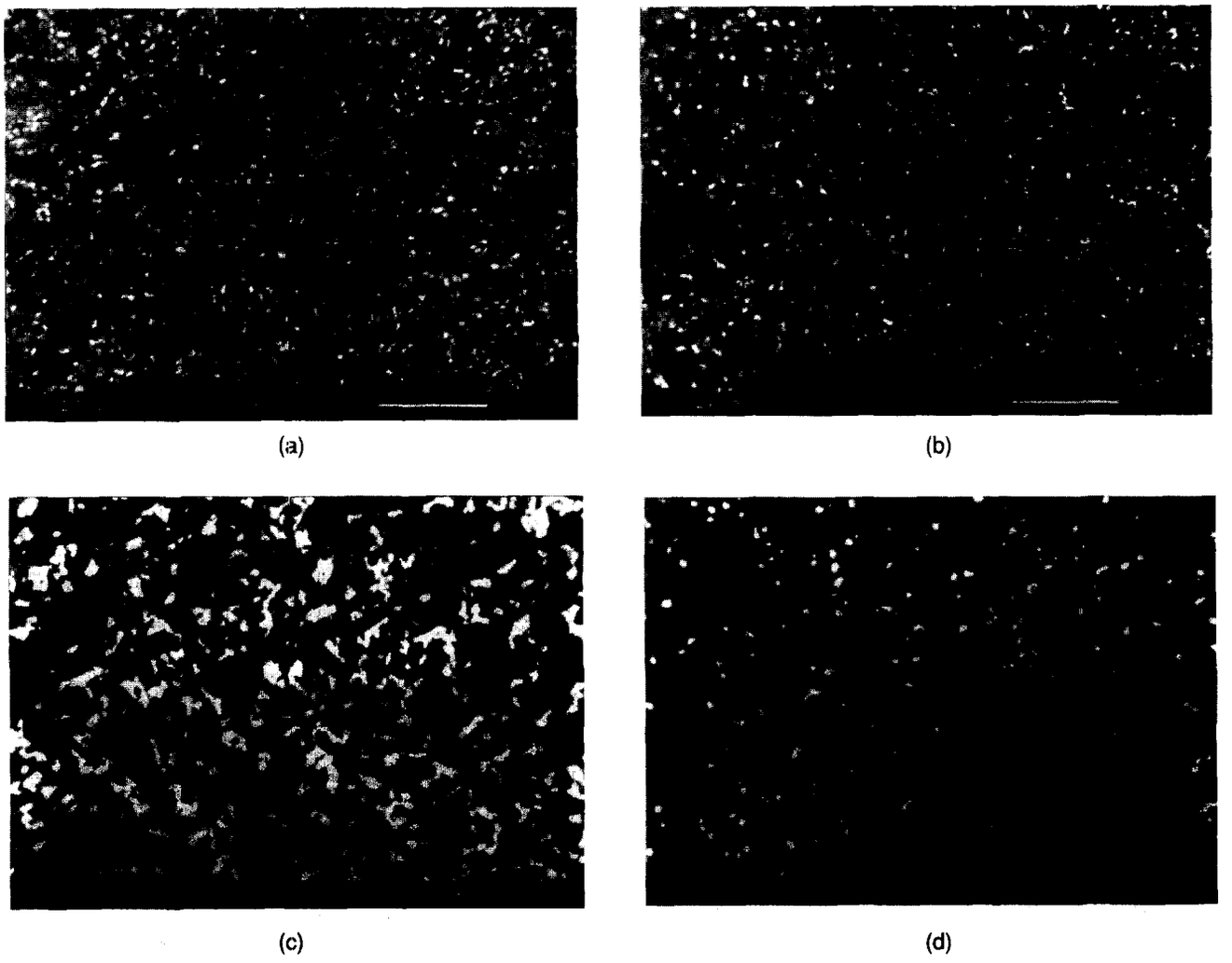

Fig. 12. Back-scattered SEM micrographs of as-sintered samples of (a) Nd5, (b) Dy5 and after heat-treatment at 1450°C for 168 h (c) Nd5, (d) Dy5.

Table 5. X-ray results for sintered and heat-treated Nd5 and Yb5 samples with 10% and 20% of extra glassy phase

Sample	*HT time (h)*	*α'(%)*	*β'(%)*	*Other*
Nd5G10	Sint	ms(77)	mw(23)	21R(w), M'(w)
	24	m(53)	m(47)	21R(w), M'(mw), A(mw)
	168	0	vs(100)	21R(mw), M'(m), A(m)
	720	0	vs(100)	21R(mw), M' (ms), A(m)
Nd5G20	Sint	ms(65)	mw(35)	21R(w), M(mw)
	24	m(48)	m(52)	21R(w), M'(m), A(mw)
	168	0	vs(100)	21R(mw), M'(ms), A(m)
	720	0	vs(100)	21R(mw), M'(vs), A(ms)
Yb5G10	Sint	vs(100)	0	21R(vw), J(w)
	24	vs(100)	0	21R(vw), G(mw), J(mw)
	168	vs(100)	0	21R(w), G(m), J(m)
	720	vs(100)	0	21R(mw), G(m), J(ms)
Yb5G20	Sint	vs(100)	0	21R(vw), J(mw)
	24	vs(100)	0	21R(vw), G(m), J(ms)
	168	vs(100)	0	21R(w), G(m), J(ms)
	720	vs(100)	0	21R(mw), G(m), J(s)

Note: for X-ray peak intensities, s=strong, m=medium, w=weak, v=very; numbers in parentheses are relative percentages of α- and β-sialon phases. α' and β' = α and β-sialons 21R=sialon polytypoid; M'=N-melilite solid solutions ($Nd_2Si_{3-x}Al_xO_{3+x}N_{4-x}$); G=$Yb_3Al_5O_{12}$; J=$Yb_4Si_2O_7N_2$, A=$NdAlO_3$.

grains, and as a result, the boundaries between adjacent α-sialon grains are almost invisible, giving the matrix a very uniform appearance. In contrast, the neodymium sample, even though there is much more second phase (because of $\alpha \rightarrow \beta$ sialon transformation), the shape is more angular, and the location of glassy pockets follows boundaries between β-sialon grains. The more wetting nature of the liquid phase in low atomic number rare earth sialon samples may be an additional factor influencing the greater extent of $\alpha \rightarrow \beta$ sialon transformation in this sample.

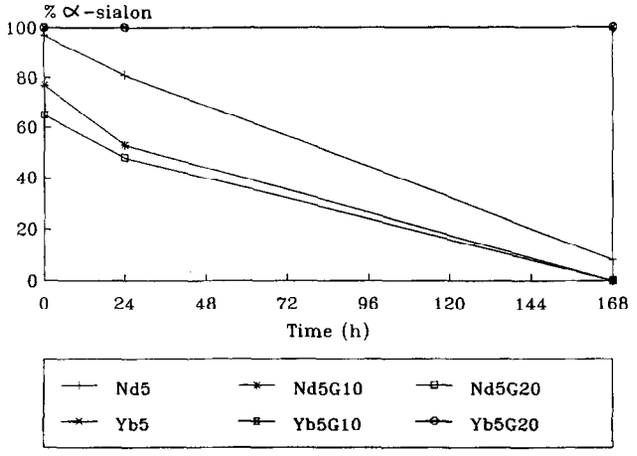

Fig. 13. α-Sialon content for Nd5 and Yb5 samples with 10% and 20% of glassy phase varying heat-treatment time at 1450°C.

In Section 3.1, the effect of the amount and viscosity of the liquid phase in promoting $\alpha \rightarrow \beta$ sialon transformation has been clearly shown by adding extra glass powder to the starting composition. To further observe this effect, 10% and 20% of glass powders with an overall composition Ln:Si:Al = 1:1:1 and O:N = 6:1 were also added to the Nd5 and Yb5 starting compositions. X-ray results of the final products after sintering and heat-treatment are given in Table 5 and Fig. 13. The amount of α-sialon reduced to 77% with 10% of glass powder addition and 65% with 20% of glass powder addition to the original Nd5 composition, which gave 97% α-sialon under similar conditions (see Table 4), with significant amount of M'-phase also observed after sintering. The rate of transformation and also the amount of M'-phase produced increased during heat-treatment

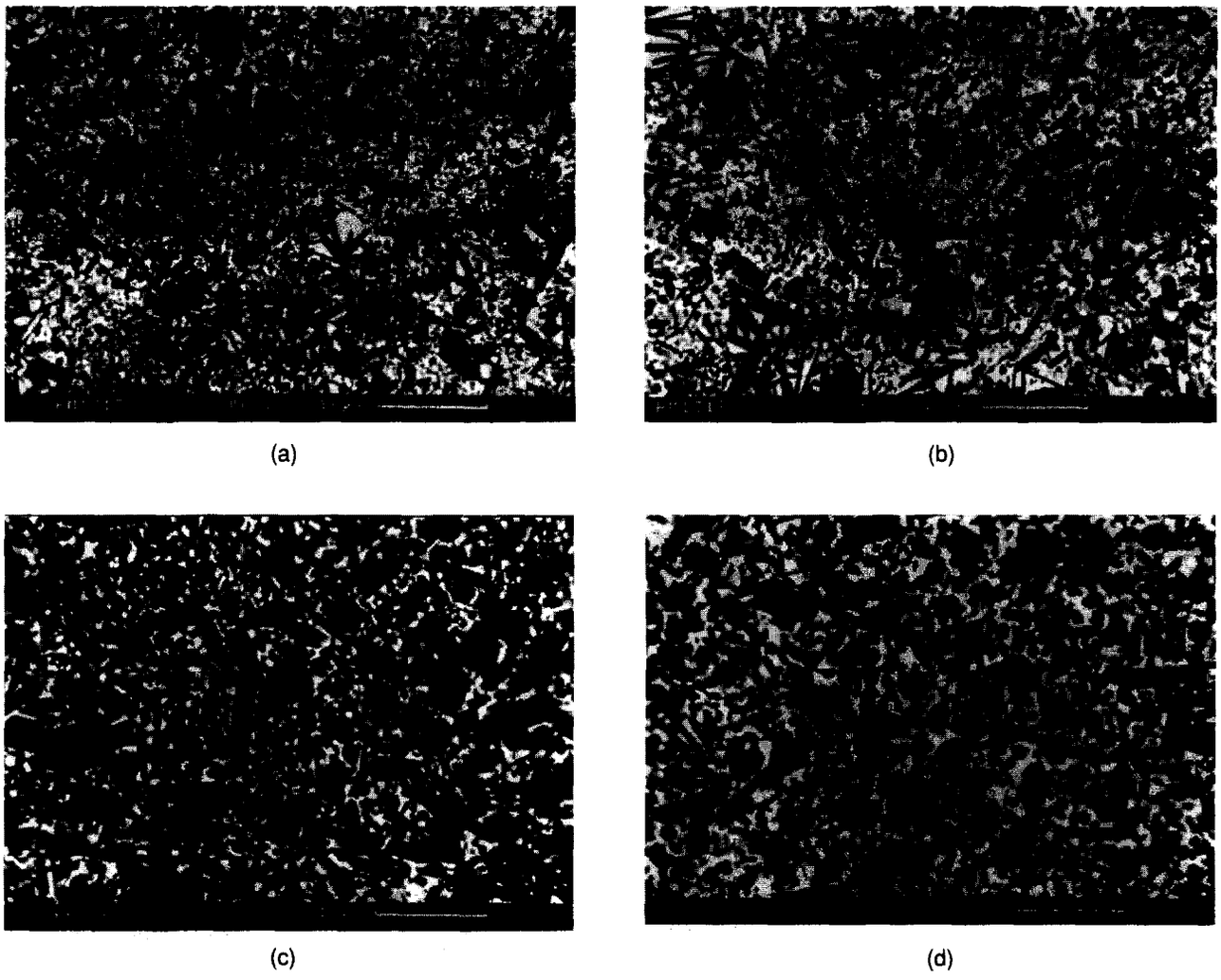

Fig. 14. Back-scattered SEM micrographs of fast-cooled samples (a) 90% Nd5 + 10% glass, (b) 80% Nd5 + 20% glass, (c) 90% Yb5 + 10% glass, (d) 80% Yb5 + 20% glass and samples after heat-treatment at 1450°C for 168 h (e) 90% Nd5 + 10% glass, (f) 80% Nd5 + 20% glass, (g) 90% Yb5 + 10% glass, (h) 80% Yb5 + 20% glass.

similar to previous observations for the Yb3 sample containing excess glass. However, additions of the same glass powder to the Yb5 sample did not show the same effect and even after 720 h (one month) of heat treatment, there was no sign of any transformation. The only difference in the Yb5 sample with extra glass additions was that the amount of crystalline phases (garnet and J-phase) increased with increasing heat-treatment time. In addition, in all samples containing excess glass, unit cell dimensions of α-sialon slightly decreased during the first seven days of heat-treatment. Further details are given elsewhere.[15]

Back-scattered SEM images in Fig. 14 also clearly showed that there was no effect on the amount and viscosity of the liquid phase in the ytterbium sample. This important difference can be explained in terms of the absence of β-sialon grains after sintering. Even a very small number of β-sialon grains (for example only 5% in the Yb4 sample), act as nucleation sites for $\alpha \rightleftarrows \beta$ sialon transformation.

To understand whether β-sialon grains play a key role in promoting the transformation, 10% β-sialon with a z value of 0·8 ($Si_{5\cdot2}Al_{0\cdot8}O_{0\cdot8}N_{7\cdot2}$) was added to the Yb1 sample and material prepared in exactly the same way as described in Section 2. The X-ray results showed that 90% α- and 10% β-sialons were obtained after sintering as intended. The z value of β-sialon was also found as $\approx$0·8. Subsequent heat-treatment steps were carried out at 1450°C for 72 h and 168 h to observe $\alpha \rightarrow \beta$ sialon transformation. After the heat-treatment cycles, 25% and 52% β-sialon were observed respectively. The back-scattered SEM images of sintered and heat-treated samples (see Fig. 15) confirmed that the presence of β-sialon grains is very important and these grains might possibly act as a nucleation site for the $\alpha \rightarrow \beta$ sialon transformation. The amount and viscosity of liquid then become important factors and the overall reaction is very similar to eqn (4).

However, this explanation is only true for small ionic size sintering additives (Dy_2O_3 and Yb_2O_3) and in the case of large ionic size sintering additives (Nd_2O_3 and Sm_2O_3), transformation can proceed without any β-sialon nucleation sites but is kinetically more favourable if they are present. More details of this work are given in a separate publication.[16]

(e)

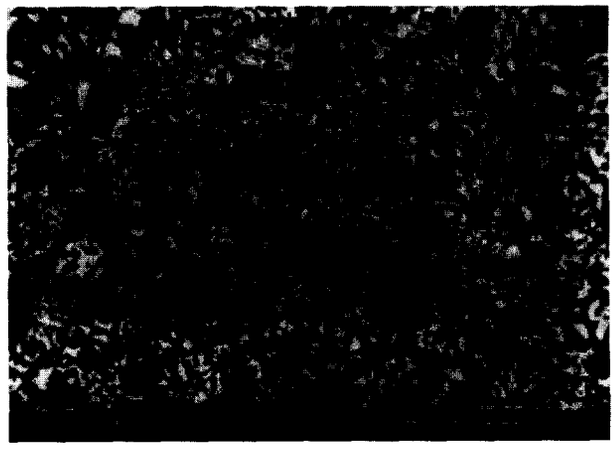

(f)

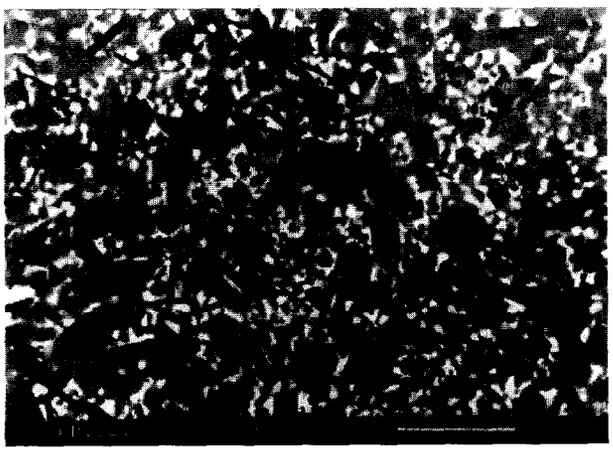

(g)

(h)

Fig. 14. *Cont.*

From these observations, it is clear that because of $\alpha \rightarrow \beta$ sialon transformation care must be exercised in the use of composite α-β sialon materials at elevated temperatures, although those materials show an excellent combination of mechanical properties between room temperature and $\approx 1000°C$.

4 Conclusions

A combination of extensive X-ray and microstructural observations on sintered and heat-treated rare-earth-densified mixed α-β sialon and α-sialon ceramic composites has shown that:

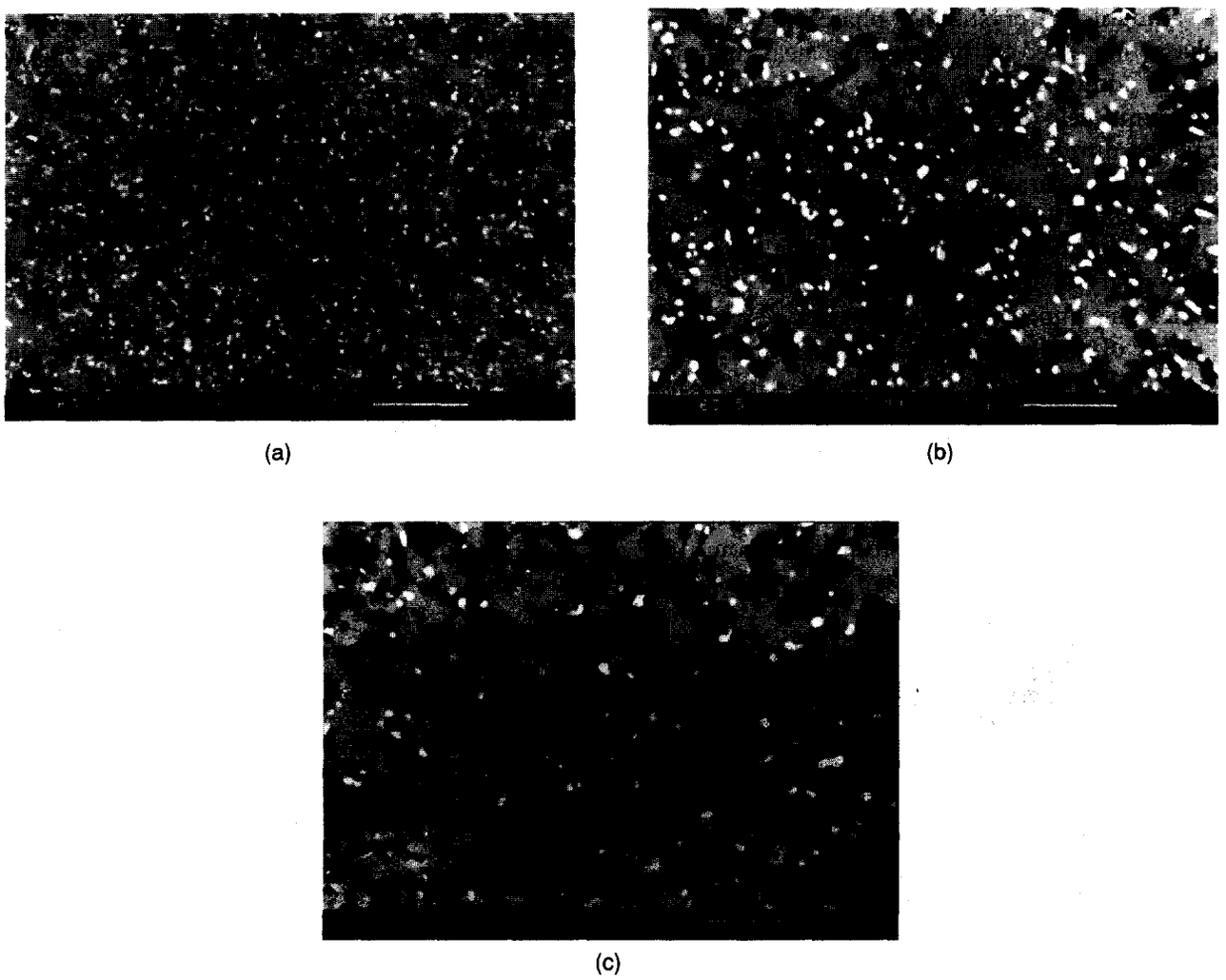

Fig. 15. Back-scattered SEM micrographs of Yb5 sample with 10% β-sialon addition (a) as-sintered, (b) 72 h heat-treated and (c) 168 h heat-treated at 1450°C.

Table 6. Mechanisms influencing $\alpha \rightleftarrows \beta$ sialon transformation

Sample	*O : N ratio (%)*	*Sintering additive*	*α → β Sialon transformation*	*Driving force*		
				Ln cation size	*Amount and viscosity of liquid phase*	*β-sialon nucleation sites*
Ln1	13·7	Nd_2O_3 or Sm_2O_3	✓	✓✓✓	✓✓	✓
		Dy_2O_3 or Yb_2O_3	✓	No	✓✓✓	✓
Ln2	10·6	Nd_2O_3 or Sm_2O_3	✓	✓✓✓	✓✓	✓
		Dy_2O_3 or Yb_2O_3	✓	No	✓✓✓	✓
Ln3	9·12	Nd_2O_3 or Sm_2O_3	✓	✓✓✓	✓✓	✓
		Dy_2O_3 or Yb_2O_3	✓	No	✓✓✓	✓
Ln4	11·88	Nd_2O_3 or Sm_2O_3	✓	✓✓✓	✓✓	✓
		Dy_2O_3 or Yb_2O_3	✓	No	✓✓	✓✓✓
Ln5	10·34	Nd_2O_3 or Sm_2O_3	✓	✓✓✓	✓✓	No
		Dy_2O_3 or Yb_2O_3	No	No	No	✓✓✓

(1) The α-sialon composition in mixed α-β sialon materials is always located at the edge of the α-sialon phase region and is less stable with respect to $\alpha \rightarrow \beta$ sialon transformation than in single phase α-sialon materials prepared with compositions within the α-sialon phase region.

(2) In α-β-sialon starting compositions the ease with which the transformation proceeds depends mainly on the amount and viscosity of liquid phase present during heat-treatment.

(3) In α-sialon starting compositions prepared within or at the edge of the α-sialon phase region, the ease with which transformation proceeds depends mainly on the cation size of the sintering additive, the presence of β-sialon grains and also the amount and viscosity of liquid phase present during heat treatment.

The overall results can be summarized as shown in Table 6, where increasing numbers of ticks indicates the more dominant mechanism influencing $\alpha \rightleftarrows \beta$ sialon transformation.

Acknowledgement

One of us (H.M.) would like to acknowledge financial assistance from the Engineering and Physical Sciences Research Council (EPSRC, UK) during the course of this work.

References

1. Ekström, T. & Ingelström, I., Characterization and properties of sialon ceramics. In *Proceeding of the International Conference Non-oxide Technical and Engineering Ceramics*, ed. S. Hampshire. Elsevier Applied Science Publishers, London, 1986, pp. 231–253.
2. Cao, G. Z., Metselaar, R. & Ziegler, G., Microstructure and properties of mixed α-β sialons. In *4th International Symposium on Ceramic Materials and Components for Engines*, ed. R. Carlsson, T. Johansson & L. Kahlman. Elsevier Applied Science Publishers, London, 1992, pp. 188–195.
3. Mandal, H., Thompson, D. P. & Ekström, T., Reversible $\alpha \rightleftarrows \beta$ SiAlON transformation in heat-treated sialon ceramics. *J. Eur. Ceram. Soc.*, **12** (1993) 421–429.
4. Mandal, H., Thompson, D. P. & Ekström, T., Optimization of sialon ceramics by heat treatment. In *Third Euro-Ceramics*, Vol. 3, ed. P. Duran & J. F. Fernandez. Faenza Editrice Iberica S.L., Spain, 1993, pp. 385–390.
5. Mandal, H., Thompson, D. P., Sun, W. Y. & Ekström, T., Mechanical property control of rare earth oxide densified α-β sialon transformation. In *5th International Symposium on Ceramic Materials and Components for Engines*, ed. D. S. Yan, X. R. Fu & S. X. Shi. World Scientific Publisher, Singapore, 1995, pp. 441–446.
6. Mandal, H. & Thompson, D. P., Mechanism of $\alpha \rightleftarrows \beta$ sialon transformation. In *Fourth Euro-Ceramics*, ed. G. Galassi. Gruppo Editoriale Faenza Editrice S.p.A., Faenza, Italy, pp. 327–334.
7. Mandal, H. & Thompson, D. P., Effect of type of rare earth oxide additive on the design of sialon ceramics. In *Fourth Euro-Ceramics*, ed. G. Galassi. Gruppo Editoriale Faenza Editrice S.p.A., Faenza, Italy, pp. 273–280.
8. Morand, C., Mandal, H. & Thompson, D. P., Evaluation of $\alpha \rightleftarrows \beta$ sialon transformation temperatures for Ln-doped α-sialons. To be published.
9. Mandal, H., Thompson, D. P. & Ekström, T., Heat treatment of Ln–Si–Al–O–N glasses. In *Proceeding of 7th Irish Materials Forum Conference, IMF7, Key Engineering Materials*, 92–94, ed. M. Buggy & S. Hampshire. Trans. Tech Publications, Switzerland, 1992, pp. 187–203.
10. Liddell, K., X-ray analysis of nitrogen ceramic phases. MSc thesis, University of Newcastle upon Tyne, UK, 1979.
11. Sun, W. Y., Tien, T. Y. & Yen, T. S., Solubility limits of α'-sialon solid solutions in the systems Si, Al, Y/N, O. *J. Am. Ceram. Soc.*, **74** (1991) 2547–2550.
12. Mandal, H., Camuşcu, N. & Thompson, D. P., Comparison of the effectiveness of rare earth sintering additives on the high temperature stability of α-sialon ceramics. *J. Mater. Sci.* (1995), accepted for publication.
13. Cheng, Y. B. & Thompson, D. P., Aluminium-containing nitrogen melilite phase. *J. Am. Ceram. Soc.*, **77** (1994) 143–148.
14. Menon, M. & Chen, I. W., Reaction densification of α-sialon: 1, Wetting behaviour and acid-base reactions. *J. Am. Ceram. Soc.*, **78**[3] (1995) 545–552.
15. Mandal, H., Thompson, D. P., Liu, Q., Gao, L. & Yan, D. S., High Temperature stability of α-sialon ceramics containing excess glass. Submitted to *J. Eur. Solid State Inorganic Chemistry* (1995).
16. Mandal, H. & Thompson, D. P., Enhancement of $\alpha \rightarrow \beta$ sialon transformation by additions of β-sialon nuclei, to be published (1995).